Supplementary Information

Protomers of DNA-binding dye fluoresce different colours: intrinsic photophysics of Hoechst 33258

JoAnn C. Chen, and Rebecca A. Jockusch*
Department of Chemistry, University of Toronto
80 St. George Street, Toronto, ON Canada L5B 4M7

*Corresponding Author: email: rebecca.jockusch@utoronto.ca

Submitted to Physical Chemistry Chemical Physics, April 2019

Contents

Supporting Figures

Fluorescence, Photodissociation (PD) and Electron Photodetachment (ePD) in a Quadrupole Ion Trap

Table S1. Summary of experimental parameters for fluorescence experiments.

	1+ Excitation Spectrum	1+ Emission Spectrum	1+ Fluorescence Lifetime	2+ Emission Spectrum
MS^n	MS^4	MS^4	MS^4	MS^3
ICC ($\times 10^5$)	0.6 - 2.1	1.0 - 2.0	1.0 - 2.3	0.6 - 1.0
q_z	0.82	0.82	0.82	0.82
$P_{He,trap}$ ($\times 10^{-3}$ mbar)	1.1	1.4 - 1.6	1.2	2.2
t_{ex} (s)	3.10	3.10	3.10	1.60
λ_{ex} (nm)	350 - 460	350	420	430
$\sum\lambda$ (nm)	540 - 610			
P (mW)	1.0	1.0	4.0	2.6
Pulse Energy (pJ/pulse)	13	13	50	33
Filter[†]	460LP	360LP	440LP	440LP

[†]long-pass (LP) filter

Table S2. Summary of experimental parameters for photodissociation (PD) and electron photodetachment (ePD) experiments

	1+ PD Action Spectrum	1+ PD Power Dependence	2+ PD Action Spectrum	2+ PD Power Dependence	dsDNA-H33258 ePD Action Spectrum
MS^n	MS^4	MS^4	MS^3	MS^3	MS^2
ICC ($\times 10^4$)	1.6 - 8.0	1.6 - 8.0	1.0 - 3.0	4.0 - 5.0	2.0 - 4.0
q_z	0.27	0.27	0.54	0.54	0.23
$P_{He,trap}$ ($\times 10^{-3}$ mbar)	1.1	1.1	1.6	1.6	1.5
t_{ex} (s)	3.10	3.10	1.00	0.50	1.00
λ_{ex} (nm)	350 - 475	350, 365, 393	350 - 430	350	348 - 400
P (mW)	4.0	0.50 - 105	0.50	0.40 - 39.1	0.60
Pulse energy (pJ/pulse)	50	6.3 - 1310	6.3	5.0 - 489	7.5

The pressure of helium buffer gas within the ion trap ($P_{He,trap}$) is monitored externally, away from the ion-trapping region. Bian *et al.* estimated the helium gas flow rate to be ~2.5 L s^{-1}, which results in a correction factor of ~140 between the actual pressure of helium in the trap and the pressure reading.[1]

Steady State Fluorescence of H33258

Gas-phase Excitation Spectrum of H33258 1+

All spectra for trapped ions were background-corrected. Background spectra were collected by not trapping any ions in the quadrupole ion trap while the laser beam was blocked. For one data point, three background-subtracted spectra were summed together to improve S/N, then integrated under the curve from 540 nm to 610 nm to extract a measure of fluorescence intensity. All points collected within the same day were normalized by the sum of fluorescence intensity at 395 nm and 400 nm for that day. The spectrum reported in the paper was averaged over multiple days, and errors bars (standard deviations of the mean) are only shown for wavelengths with 3 or more repeat measurements. A 5-points, second-order Savitzky-Golay smoothing was performed.

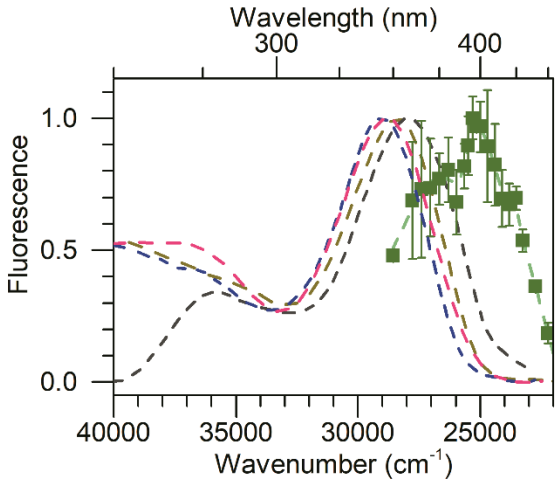

Figure S1. Gas-phase excitation spectrum of H33258 1+ is red-shifted relative to excitation maxima in 1:1 MeoH:Water pH 4.1 (pink), 1:1 MeOH:Water pH 6.8 (blue), acetonitrile (dark yellow) and DMSO (dark gray).

Gas-phase Emission Spectra of H33258 1+

Fluorescence emission from H33258 1+ were corrected with background spectra between each signal acquisition cycle (22.48 s * 8 or 10 accumulations), then added together to improve signal-to-noise in order to distinguish spectral features.

Solution-phase Fluorescence

Solution-phase spectra in Figure 2 of the main manuscript were acquired on the LS 55 spectrometer while spectra in Figure S3 were acquired on the LS 50B spectrometer. Raw data were smoothed with 75-points (Fig. S2) or 25-points (Fig. S3) second-order Savitzky-Golay functions. The concentration of H33288 was 0.5 µM, and all measurements were taken at ambient temperature.

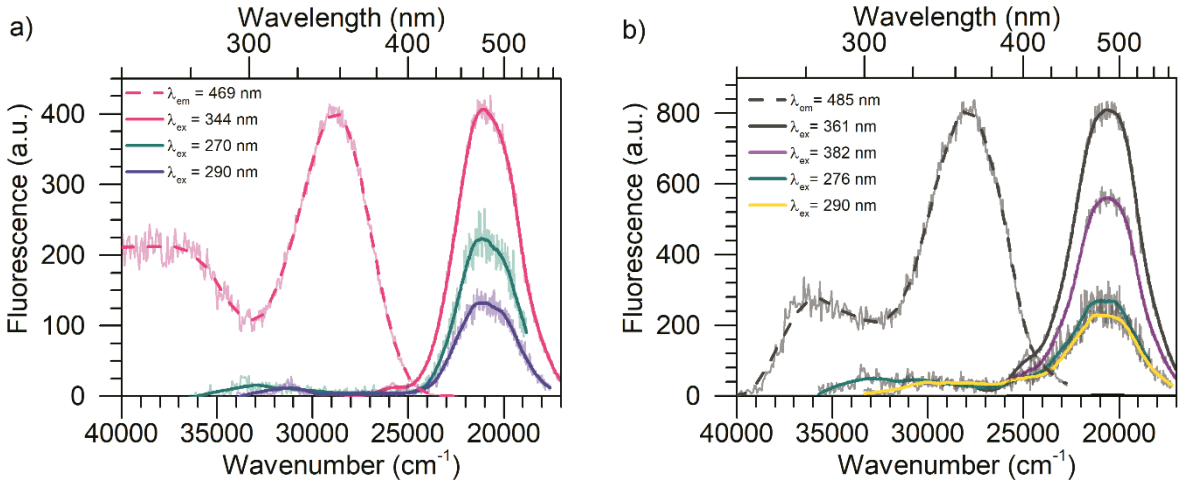

Figure S2. Solution-phase excitation (dashed) and emission (solid) spectra of H33258 measured in 1:1 MeOH:Water at pH 4.1 (a) and neat DMSO (b) at various excitation wavelengths.

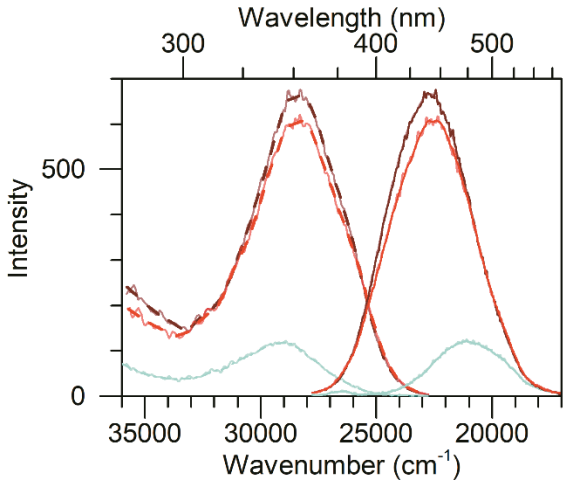

Figure S3. Solution-phase excitation (dashed) and emission (solid) spectra of free H33258 in deionised water (light cyan), and complexed to ds$(CG)_2A_2T_2(CG)_2$ (red) and ds$CGCA_3T_3GCG$ (dark red). The dye concentration was 0.5 µM in all measurements.

Table S3. Summary of Fluorescence excitation maxima, emission maxima and Stokes shifts of H33258 *in vacuo* and in select solutions

	λ_{ex} (nm) (relative intensity)	λ_{em} (nm)	$\Delta\tilde{\nu}$ (cm^{-1})
1+ (Gas)	397.5	394 523	6200
2+ (Gas)	N/A	492	undetermined
1:1 MeOH:water (pH 4.1)	347, 263[†] (1.9:1)	475 (λ_{ex} = 344 nm)	7770
1:1 MeOH:water (pH 6.8)	344	471	7840
Water	344	473	7970
DMSO	357, 279 (2.9:1)	486 (λ_{ex} = 361 nm)	7440
CH_3CN	353	500	8330

[†]poor signal-to-noise

Time-Resolved Fluorescence of H33258 1+

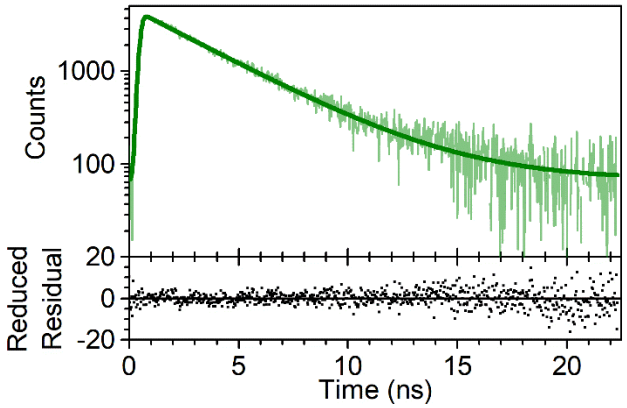

Figure S4. Time-resolved fluorescence decay of H33258 1+ resulted in a lifetime constant of 3.48 ± 0.06 ns for the major emission feature at 523 nm using a 440 nm long-pass filter. Fit analysis is presented in Table S4.

Table S4. Fit analysis of cumulated fluorescence decay curve, and individual measurements from separate days. The function below was used for the fit. It is a convolution of an exponential decay with a Gaussian of full-width-half-max w_0 to represent the instrumental response function. A is the amplitude, and τ is the lifetime constant.

$$y = y_0 + \left\{ \left(\frac{1}{4}\right) A\sqrt{\pi} \left(e^{\left(\frac{w_0^2}{\tau^2\, ln(2)}\right)} \right)^{\frac{1}{16}} w_0 * \frac{erf\left[\left(\frac{1}{4}\right)\frac{8\, ln(2)\,(x - x_0)\tau - w_0^2}{\sqrt{ln(2)}\, w_0 \tau} + 1\right]}{\sqrt{ln(2)}\, e^{\frac{x - x_0}{\tau}}} \right\}$$

	Cumulated	Trial 1	Trial 2	Trial 3
A (counts)	12223	3622	3555	7787
w_0 (ns)	0.321	0.291	0.343	0.28
τ (ns)	3.48	3.63	3.58	3.41
Adj. R^2	0.993	0.990	0.990	0.982

Photodissociation of H33258 1+

Table S5. Fit parameters for Survivor Yield at 350, 365 and 393 nm (Fig. 2a in main article) and 452 nm using a cubic exponential function where *P* is laser power in mW.

$$y = y_0 + (1 - y_0)e^{(-aP - bP^2 - cP^3)}$$

λ_{ex} (nm)	350	365	393	452
y_0	0.0053	0.0566	0.1412	0.2320
a (restricted ≤ 0)	0	0	0	0
b	0.0857	0.0468	0.0333	0.1846
c	0.0062	0.0075	0.0146	0
Adj. R^2	0.998	0.997	0.999	0.997

Table S6. Photodissociation fragments from H33258 1+

Chemical Formula	Exact Mass	Measured m/z*
$C_{24}H_{20}N_5O^+$	394.17	394.3
$C_{22}H_{18}N_5O^{2\bullet+}$	368.15	368.2
$C_{23}H_{19}N_5^{3\bullet+}$	365.16	365.2
$C_{21}H_{16}N_5O^{2\bullet+}$	354.13	353.2
$C_{22}H_{17}N_5^{3\bullet+}$	351.15	351.2
$C_{21}H_{17}N_5^{\bullet+}$	339.15	339.2
$C_{20}H_{14}N_4O^{\bullet+}$	326.12	326.2
$C_{19}H_{13}N_4^{4\bullet+}$	297.11	297.2
$C_{14}H_{12}N_4^{3\bullet+}$	236.11	236.2

* m/z measured using a QIT mass spectrometer without recent mass calibration

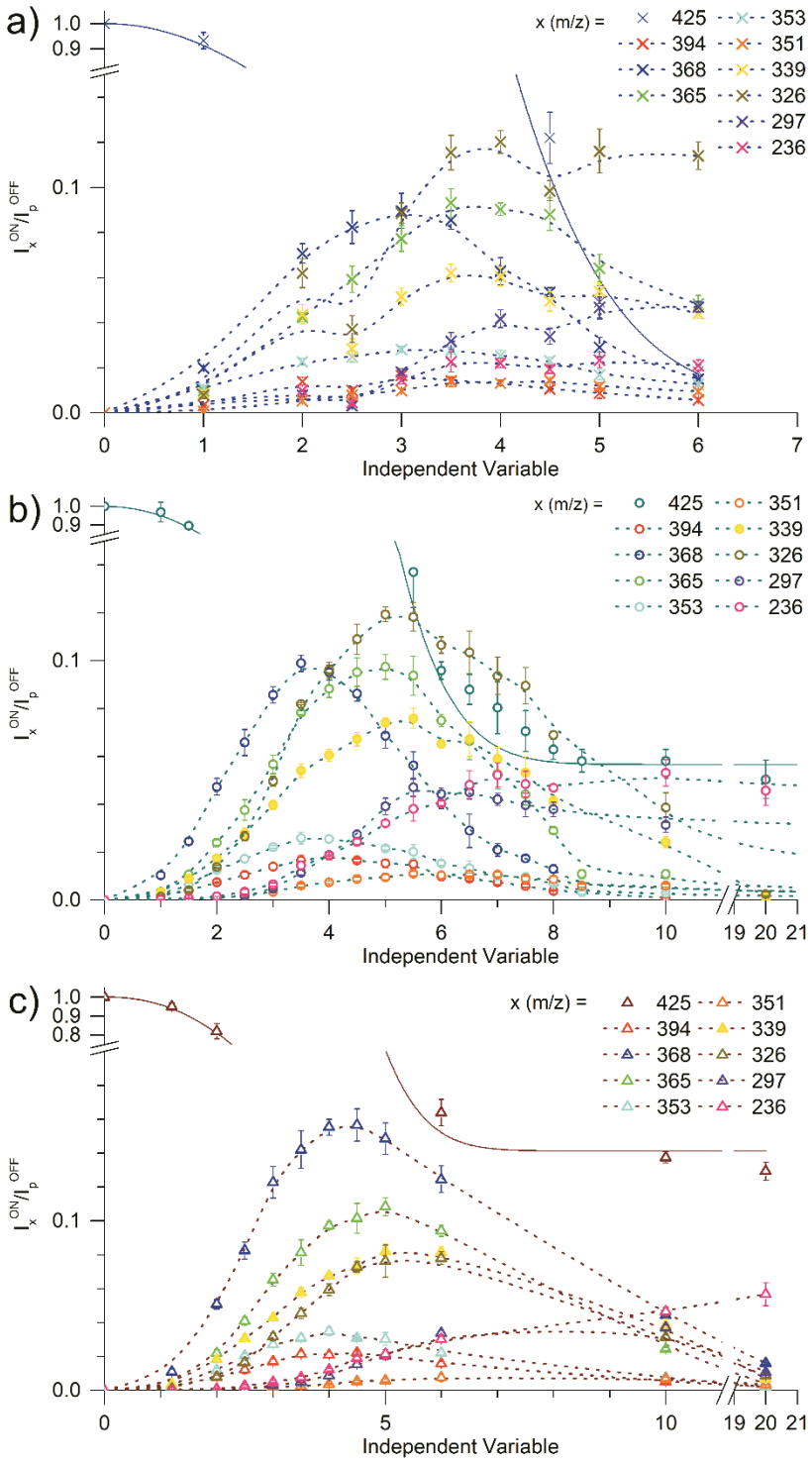

Figure S5. Power dependence of H33258 1+ photodissociation and product yields at 350 nm (a), 365 nm (b) and 393 nm (c). Errors are standard deviations from 4 sequential acquisitions.

Photodissociation of H33258 2+

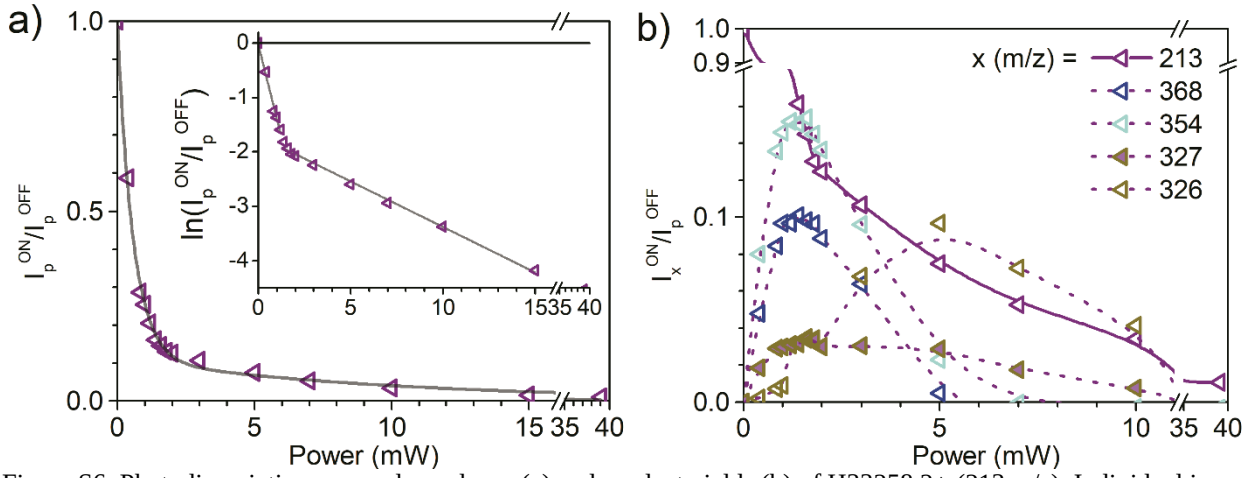

Figure S6. Photodissociation power dependence (a) and product yields (b) of H33258 2+ (213 m/z). Individual ion populations were subjected to 0.65 s of laser irradiation at 350 nm. Power dependence (a) were best-fit with a biexponential decay function. The inset, in which the natural logarithm of the remaining precursor ion is plotted, shows two separate linear fits from 0-1.20 mW and 1.2-15.0 mW. Breakdown curves (b) demonstrate that the protonated N2 is removed to yield mono-protonated fragments at 368 and 354 m/z. The entire piperazine ring (protonated) is removed to yield the 327 m/z fragment.

Table S7. Fit Parameters for photodissociation of H33258 2+ fit with biexponential decay as shown in Figure S6. *P* is laser power in mW.

$$y = A_1 e^{-b_1 P} + A_2 e^{-b_2 P}$$

	Fitted Value
A_1	0.8968
b_1	1.752
A_2	0.1128
b_2	0.1049
R^2	0.997

Table S8. Photodissociation Fragments from H33258 2+

Chemical Formula	Exact Mass	Measured m/z[†]
$C_{22}H_{18}N_5O^{2\bullet+}$	368.15	368.3
$C_{21}H_{16}N_5O^{+}$	354.13	354.3
$C_{20}H_{15}N_4O^{+}$	327.12	327.2
$C_{20}H_{14}N_4O^{\bullet+}$	326.12	326.3

[†] m/z measured using a QIT mass spectrometer without recent mass calibration

DFT Calculations for H33258 1+ and 2+

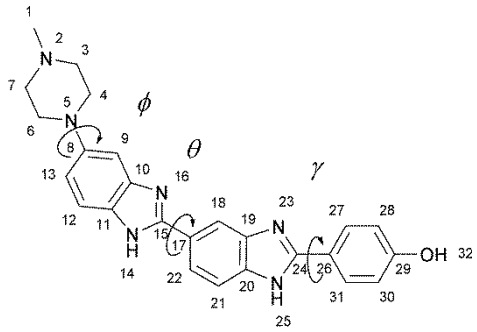

Scheme S1. Structure of neutral H33258.

Dihedral angles are reported in Tables S9-12. The angles ϕ, θ and γ were assigned as follows:

ϕ = <(C4/C6-N5-C8-C9)

θ = <(N16-C15-C17-C18)

γ = <(N23-C24-C26-C27/C31)

C4 and C6 are indistinguishable, but the conformation of the piperazine ring changes among structures, so both dihedral angles are reported.

Table S9. Ground state relative energies and dihedral angles for 1+ charge state optimised at B3LYP/6-31G(d)

Structure	Protonation Site	B3LYP/6-31G(d)				B3LYP/6-311+G(d,p)// B3LYP/6-31G(d)
		ΔE (kJ/mol)	ϕ	θ	γ	ΔE (kJ/mol)
H-pipN2-I	N2	25.9	123.6/-16.9	12.3	4.7	24.8‡
H- pip1-b	N2	39.1	59.7/-157.4	12.8	-3.9	38.9
H-pipN2-II	N2	29.0	123.1/-17.6	-169.0	2.4	28.8‡
H- pip1-d	N2	35.9	-157.2/59.8	-167.7	-4.4	35.1
H-pipN5-I	N5	0	116.1/-116.0	-7.9	-2.0	0‡
H-pip2-b	N5	47.3	78.6/-51.6	-7.4	-0.2	
H-pipN5-II	N5	8.9	-64.0/63.9	171.9	2.1	9.0‡
H-pip2-d	N5	38.5	128.7/-101.1	172.4	-1.4	41.0
H-bz1-aI	N16	124.0	-165.2/-14.6	-180.0	0.0	
H-bz1-aII	N16	127.8	173.9/-37.1	0.5	0.0	
H-bz1-bI	N14	120.9	32.3/-176.7	-0.2	0.0	
H-bz1-bII	N14	124.3	32.5/-176.4	179.9	0.0	
H-bz2-a	N23	164.5	-130.6/8.4	176.0	0.1	
H-bz2-bI	N25	160.6	-129.8/8.6	-179.2	0.0	
H-bz2-bII	N25	154.1	-7.2/135.7	-0.5	0.0	
H-phe-aI	O32	264.1	-125.9/10.4	6.5	-0.1	
H-phe-aII	O32	260.7	-9.1/129.4	174.3	0.1	

‡ Geometry selected for re-optimization at the B3LYP/6-311+G(d,p) level. See Table S10.

Table S10. Ground state relative energies and dihedral angles for 1+ charge state optimised at B3LYP/6-311+G(d,p)

Structure	Protonation Site	B3LYP/6-311+G(d,p)			
		ΔE (kJ/mol)	ϕ	θ	γ
H-pipN2-I	N2	25.0	125.2/-15.6	12.4	8.5
H-pipN2-II	N2	28.8	125.5/-15.6	-166.5	7.8
H-pipN5-I	N5	0	-115.9/116.2	-9.4	-6.3
H-pipN5-II	N5	9.1	-64.1/64.0	170.3	5.0

Table S11. Ground state relative energies for 2+ charge state at B3LYP/6-31G(d) level of theory

Structure	Protonation Sites	ΔE (kJ/mol)	ϕ	θ	γ
H-bz1-bz2-a	N16, N23	195.6	174.9	-179.8	0.0
H-bz1-bz2-b	N16, N25	198.5	174.9	0.4	0.0
H-bz1-bz2-c	N14, N25	211.2	9.1	180.0	0.0
H-bz1-bz2-d	N14, N23	207.8	14.8	0.0	0.0
H-pip1-bz1-aI	N2, N16	49.7	156.5	0.2	0.1
H-pip1-bz1-aII	N2, N16	46.5	158.1	-179.7	-0.1
H-pip1-bz1-bI	N2, N14	34.3	-12.9	179.9	0.0
H-pip1-bz1-bII	N2, N14	32.9	-12.6	0.1	-0.1
H-pip1-bz2-aI	N2, N23	17.5	-117.7	8.4	0.1
H-pip1-bz2-aII	N2, N23	7.9	-113.0	171.1	0.1
H-pip1-bz2-bI	N2, N25	5.5	-117.4	0.6	0.0
H-pip1-bz2-bII	N2, N25	0.0	-113.2	-179.9	0.0
H-pip2-bz2-aI	N5, N25	37.6	-64.0	11.6	0.1
H-pip2-bz2-aII	N5, N23	26.9	116.2	-170.5	0.1
H-pip2-bz2-bI	N5, N25	17.4	116.1	-180.0	0.0
H-pip2-bz2-bII	N5, N25	25.4	-64.1	0.0	0.0

Coordinates for the H33258 ligand in the solved crystal structure of H33258 complexed to $ds(CG)_2A_2T_2(CG)_2$ (PDB: 8BNA[2]) were compared with optimised gas-phase geometries at the B3LYP/6-311+G(d,p) level of theory.

Table S12. Dihedral angles of H33258 ligand complexed to Dickerson's Dodecamer (PDB: 8BNA)

Structure	Protonation Site(s)	ϕ	θ	γ
H33258 in 8BNA	not available	104.4/-115.2	36.9	0.9

TD-DFT Calculations for H33258 1+

All TD-DFT calculations were performed at the B3LYP/6-31G(d) level of theory, and molecular orbitals were generated in Gaussview 6.[3]

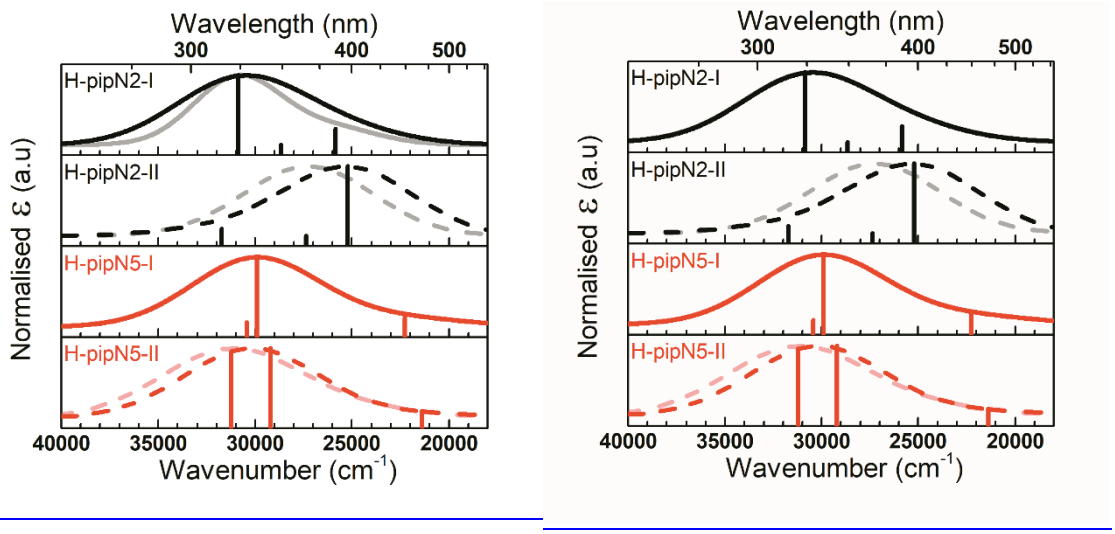

Figure S7. TD-DFT/B3LYP/6-31G(d) level electronic transition energies to the first three excited states computed at the optimised ground state geometry (translucent lines), and at the optimised S_1 geometry (opaque lines).

Table S13. Excitation energies (vertical absorption) for the first three excited states of 1+ charge state at the TD-DFT/B3LYP/6-31G(d) level calculated at the optimised ground state geometries.

Structure	Energy (nm)	Oscillator strength	Component transitions	Coefficient
H-pipN2-I	386.76	0.3146	112→113	0.69810
	348.84	0.0007	112→114	0.70258
	324.10	1.3559	111→113 112→115	0.63680 0.26536
H-pipN2-II	367.42	1.3465	112→113	0.70251
	349.77	0.0138	112→114	0.70170
	305.20	0.0066	110→113 111→113 112→115 112→120	0.44965 -0.43050 -0.26138 0.12766
H-pipN5-I	449.01	0.1104	112→113	0.70341
	334.31	0.8693	111→113 112→114 112→115	0.67290 -0.14967 0.11966
	328.56	0.0588	111→113 112→114	0.15076 0.68531
H-pipN5-II	407.16	0.1559	112→113	0.70220
	330.94	0.9054	111→113	0.69463
	304.83	0.6061	109→113 110→113 112→114	-0.10613 -0.20768 0.65373

Table S14. Excitation energies at the optimised S_1 geometries (simulating fluorescence transitions) for the first three excited states of 1+ charge state at the TD-DFT/B3LYP/6-31G(d) level.

Structure	Energy (nm)	Oscillator strength	Component transitions	Coefficient
H-pipN2-I	386.77	0.3146	112⟶113	0.69808
	348.86	0.0007	112⟶114	0.70258
	324.11	1.3551	111⟶113 112⟶115	0.63697 0.26491
H-pipN2-II	396.69	1.5869	112⟶113	0.70329
	362.46	0.0072	112⟶114	0.70173
	315.08	0.1670	110⟶113 111⟶113 112⟶115	0.42735 0.24542 -0.49201
H-pipN5-I	449.01	0.1103	112⟶113	0.70340
	334.31	0.8690	111⟶113 112⟶114 112⟶115	0.67297 -0.14968 0.11924
	328.56	0.0592	111⟶113 112⟶114	0.15065 0.68535
H-pipN5-II	468.10	0.0901	112⟶113	0.70396
	342.43	0.8574	111⟶113	0.69351
	320.28	0.8227	110⟶113 112⟶114	-0.30057 0.62083

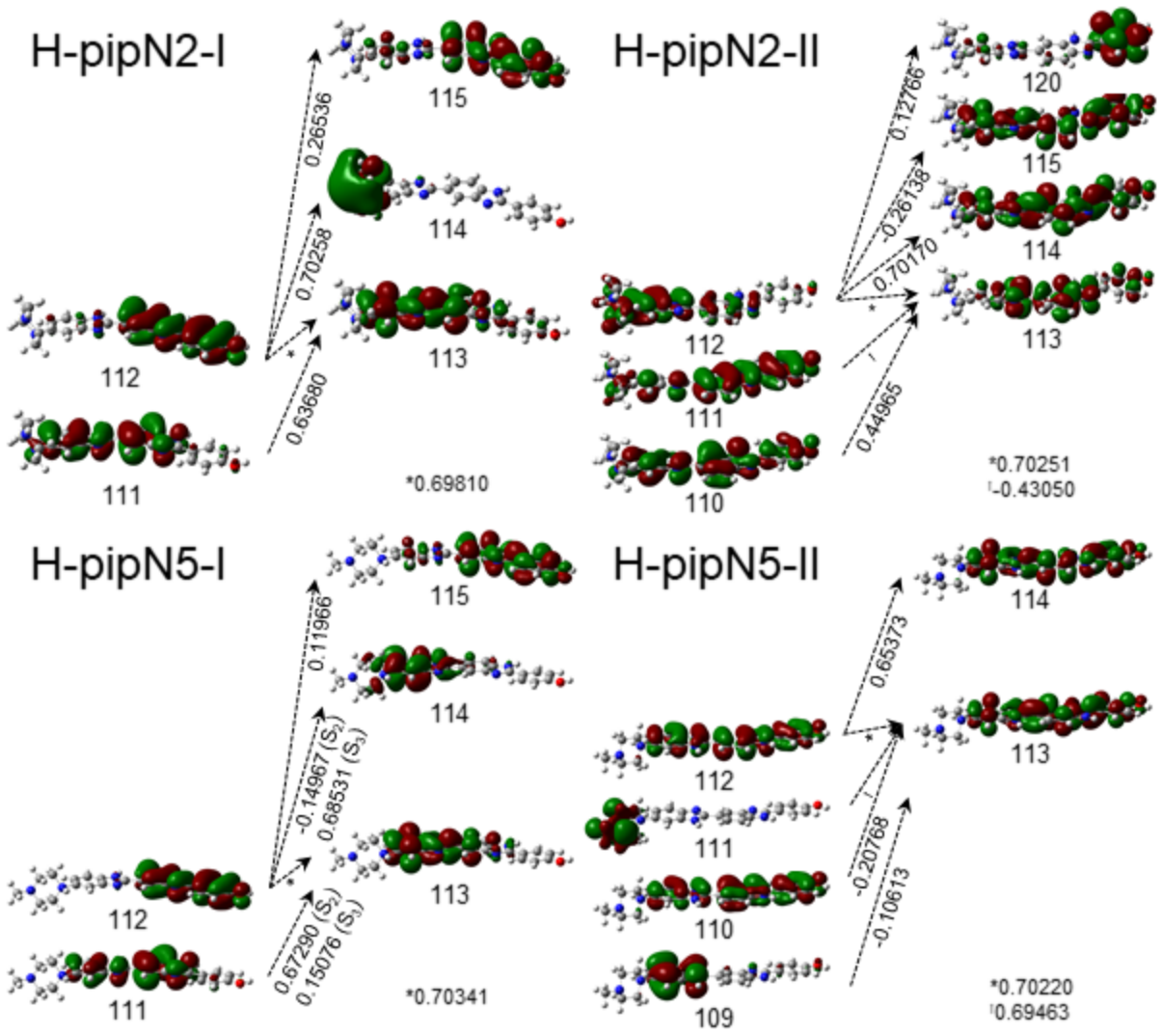

Figure S8. Component transitions for the vertical transitions to the first three excited states for H-pipN2-I, H-pipN2-II, H-pipN5-I and H-pipN5-II at their optimised ground state geometries. Arrows show transitions labeled with their corresponding coefficient computed at the the TD-DFT/B3LYP/6-31G(d) level .

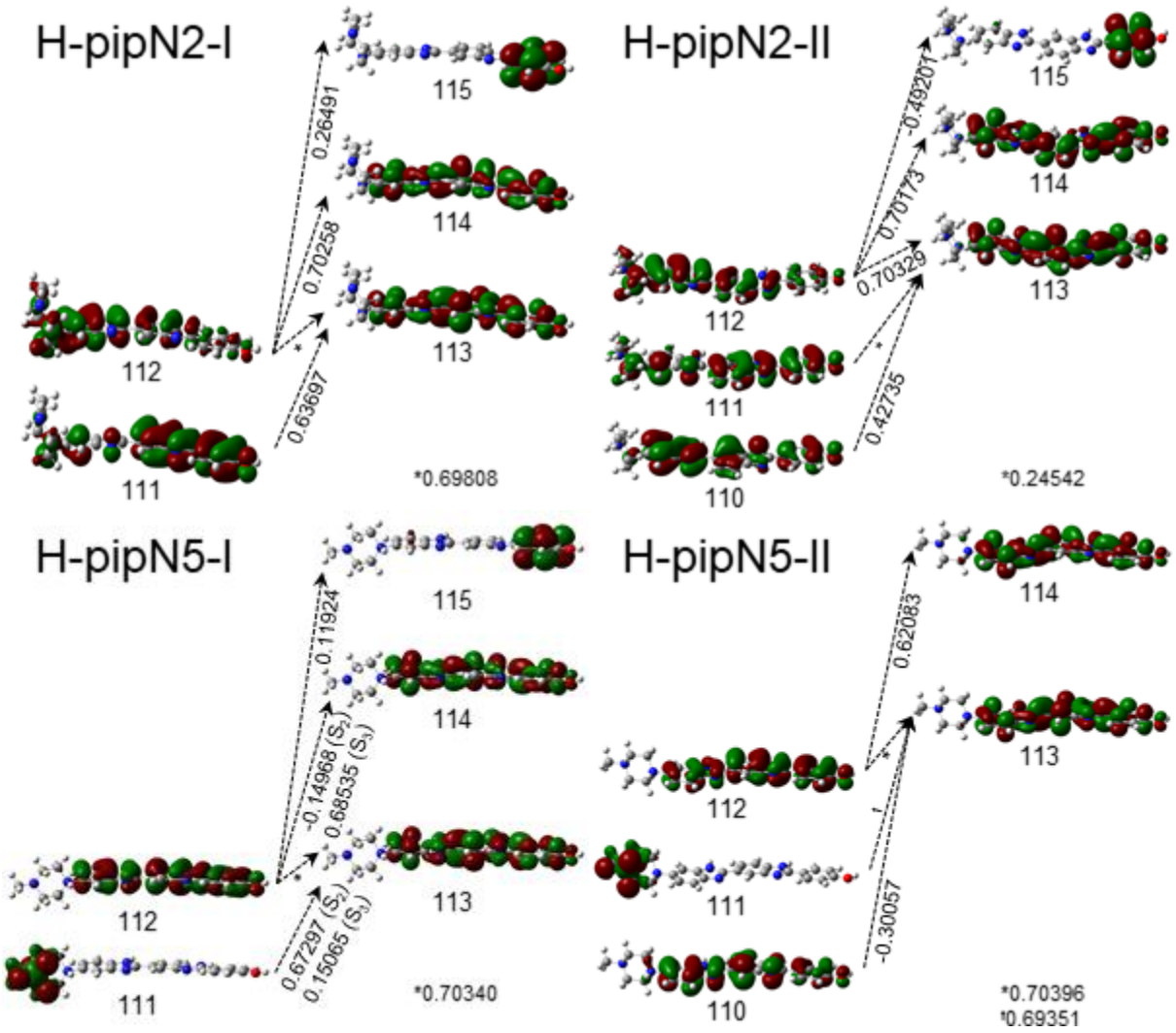

Figure S9. Component transitions for the "pseudo-fluorescence" of the optimised S_1 state of H-pipN2-I, H-pipN2-II, H-pipN5-I and H-pipN5-II are shown. Arrows show transitions labeled with their corresponding coefficient computed at the the TD-DFT/B3LYP/6-31G(d) level.

High resolution mass spectra of $ds(CG)_2A_2T_2(CG)_2$-H33258 complex

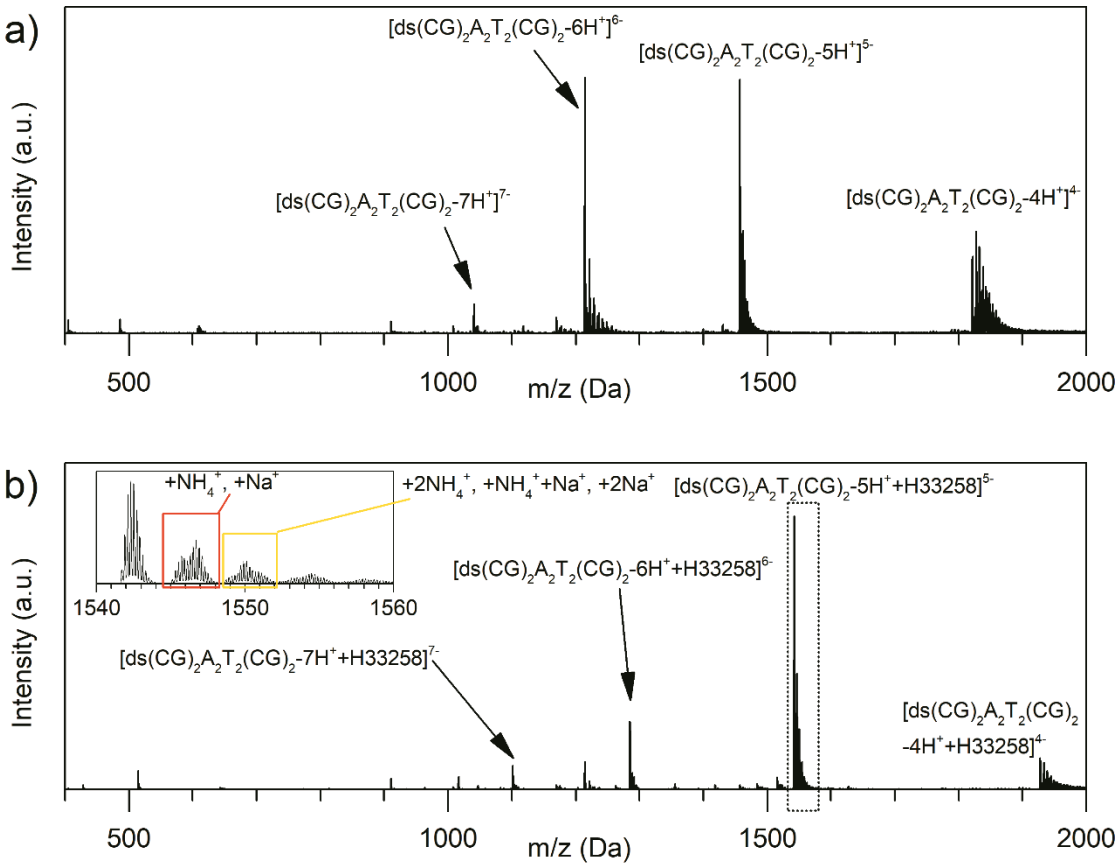

Figure S10. NanoESI-FT-ICR mass spectra of 12.5 µM $ds(CG)_2A_2T_2(CG)_2$ in 100 mM ammonium acetate without (a) and with (b) 12.5 µM H33258. Four charge states – 7-, 6-, 5- and 4- – were clearly observed for the bare dsDNA and the dsDNA-H33258 complex. A mixture of adducts containing NH_4^+ and Na^+ were observed for the bare dsDNA and dsDNA-H33258 complexes (inset in b).

Collision-induced photodissociation (CID) and electron photodetachment (ePD) of $ds(CG)_2A_2T_2(CG)_2$-H33258 complex

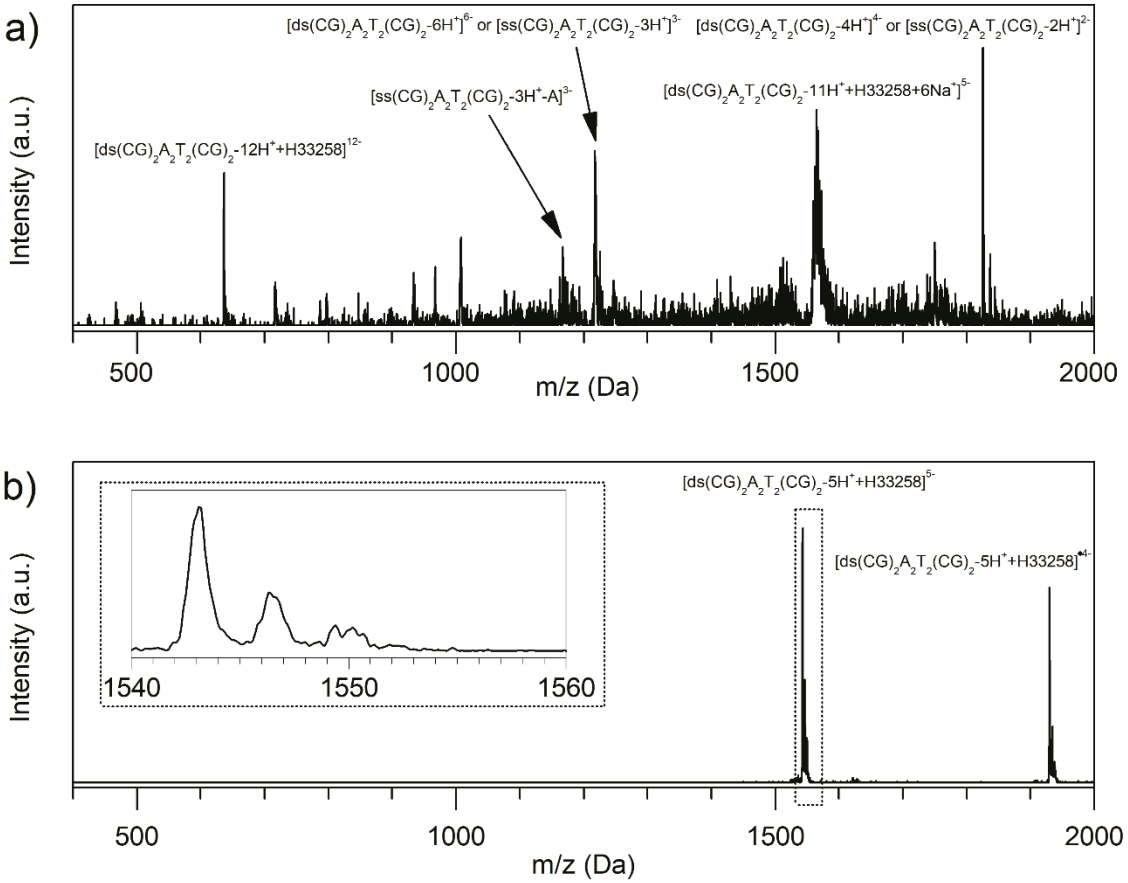

Figure S11. MS/MS spectra of $[ds(CG)_2A_2T_2(CG)_2\text{-}5H^+\text{+H33258}]^{5-}$ activated with CID and no laser irradiation (a) and activated with only 350-nm laser irradiation (b) measured on the *Esquire 3000+* QIT MS. Aside from the applied CID voltage, mass spectrometry parameters were the same as those used in ePD experiments. Ion populations selected during ePD experiments included a mixture of adducts containing one NH_4^+, one Na^+, two NH_4^+, one NH_4^+ plus one Na^+, or two Na^+ (inset in b).

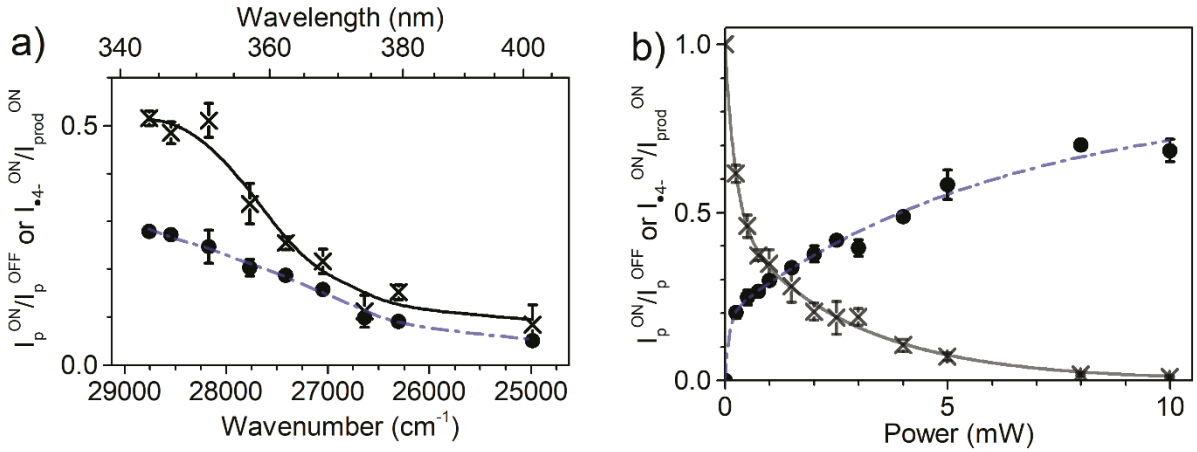

Figure S12. ePD action spectrum of $[ds(CG)_2A_2T_2(CG)_2\text{-}5H+H33258]^{5-}$ (a) represented by fraction remaining of the 5- precursor (I_p^{ON}/I_p^{OFF}) (-×-), and as %yield of the 4- radical product ion ($I_{\bullet 4-}^{ON}/I_{prod}^{ON}$) (··●-) joined with 5-pt Savitzky-Golay smooths to guide the eye. Power dependence (b) of depletion of the 5- precursor ion (-×-) and %yield of the 4- radical product (··●-) both support two-component single-photon absorption. I_p^{ON}/I_p^{OFF} is presented in the main article for direct comparison with photodissociation data.

$$\frac{I_{\bullet 4-}^{ON}}{I_{prod}^{ON}} = \frac{I_{\bullet 4-}^{ON}}{I_{\bullet 4-}^{ON} + I_{5-}^{ON}}$$

Table S15. Fit Parameters for photodissociation of $[ds(CG)_2A_2T_2(CG)_2\text{-}5H+H33258]^{5-}$ fit with a biexponential decay as shown in Figure S12b. *P* is laser power in mW.

$$y = A_1 e^{-b_1 P} + A_2 e^{-b_2 P} + y_0$$

	I_p^{ON}/I_p^{OFF}
A_1	0.5254
b_1	4.263
A_2	0.4748
b_2	0.3675
y_0	0
Adj. R^2	0.997

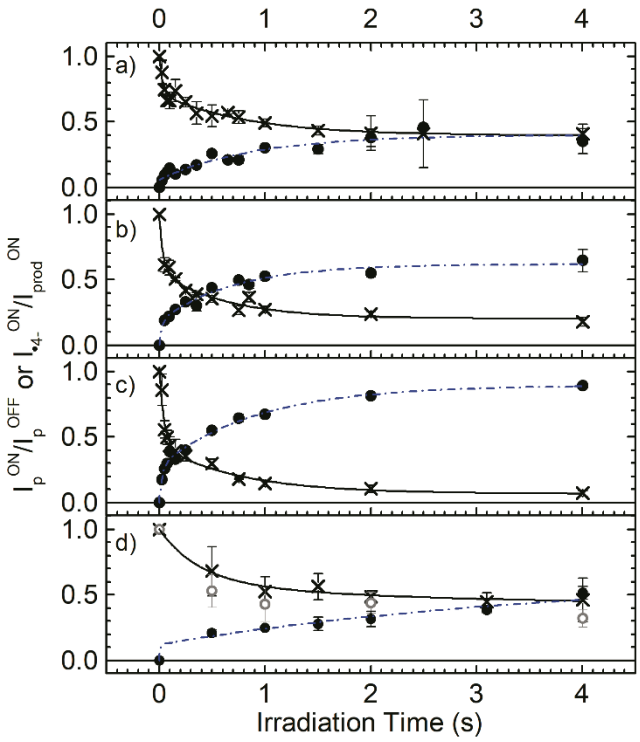

Figure S13. ePD kinetics showing depletion of the 5- complex (-x-) and %yield of the 4- radical complex (-●-) as a function of irradiation time. 350-nm light was used at 0.6 mW (a), 1.2 mW (b), 2.0 mW (c) and at 0.6 mW with low helium bath pressure (d). Normal helium bath pressure was 1.5×10^{-3} mbar, while the low helium bath pressure was 0.43×10^{-3} mbar. Translucent gray data points in (d) show depletion of the 5- complex at the normal helium bath pressure measured immediately before low pressure measurements. Depletion of the precursor ion was best-fit with a biexponential decay function (fit parameters in Table S16).

Table S16. Fit Parameters for biexponential decay function of I_p^{ON}/I_p^{OFF} in Figure S13 where t_{irr} is irradiation time in seconds.

$$y = A_1 e^{-b_1 t_{irr}} + A_2 e^{-b_2 t_{irr}} + y_0$$

Power (mW)	0.6	1.2	2.0	0.6
He bath pressure (mbar)	1.5×10^{-3}	1.5×10^{-3}	1.5×10^{-3}	0.43×10^{-3}
A_1	0.3216	0.3585	0.3652	0.3955
b_1	1.220	1.593	1.314	2.721
A_2	0.2959	0.4367	0.5988	0.1773
b_2	32.68	28.09	21.88	0.4973
y_0	0.3937	0.2017	0.0660	0.4283
Adj. R^2	0.956	0.967	0.973	0.951

References

1 Q. Bian, M. W. Forbes, F. O. Talbot and R. A. Jockusch, Gas-phase fluorescence excitation and emission spectroscopy of mass-selected trapped molecular ions, *Phys. Chem. Chem. Phys.*, 2010, **12**, 2590–2598.

2 P. E. Pjura, K. Grzeskowiak and R. E. Dickerson, Binding of Hoechst 33258 to the minor groove of B-DNA, *J. Mol. Biol.*, 1987, **197**, 257–271.

3 R. D. Dennington II, T. A. Keith and J. M. Millam, *GaussView 6.0.16*, Semichem. Inc., 2000.